Frontiers in Bioscience Landmark

Front. Biosci. (Landmark Ed) **2024**; 29(9): 318
https://doi.org/10.31083/j.fbl2909318

Original Research

Developing and Verifying an Effective Diagnostic Model Linked to Immune Infiltration in Stanford Type A Aortic Dissection

Xiaoyan Huang[1,2], Guoan Zhang[3], Yangmeng Feng[1,2], Xiangrong Zhao[1,2], Yaping Li[1,2], Fuqiang Liu[4], Yihan Dong[5], Jingying Sun[1,2], Cuixiang Xu[1,2,*]

[1]Shaanxi Provincial Key Laboratory of Infection and Immune Diseases, Shaanxi Provincial People's Hospital, 710068 Xi'an, Shaanxi, China
[2]Shaanxi Engineering Research Center of Cell Immunology, Shaanxi Provincial People's Hospital, 710068 Xi'an, Shaanxi, China
[3]Department of Cardiology Surgery, Shaanxi Provincial People's Hospital, 710068 Xi'an, Shaanxi, China
[4]Department of Cardiology, Shaanxi Provincial People's Hospital, 710068 Xi'an, Shaanxi, China
[5]Department of Graduate School, Yan'an University, 716000 Yan'an, Shaanxi, China
*Correspondence: xucuixiang1129@163.com (Cuixiang Xu)
Academic Editor: Haseeb Ahmad Khan
Submitted: 19 April 2024 Revised: 20 June 2024 Accepted: 28 June 2024 Published: 6 September 2024

Abstract

Background: The deadly cardiovascular condition known as Stanford type A aortic dissection (TAAD) carries a high risk of morbidity and mortality. One important step in the pathophysiology of the condition is the influx of immune cells into the aorta media, which causes medial degeneration. The purpose of this work was to investigate the potential pathogenic significance of immune cell infiltration in TAAD and to test for associated biomarkers. **Methods**: The National Center for Biotechnology Information (NCBI) Gene Expression Omnibus (GEO) database provided the RNA sequencing microarray data (GSE153434, GPL20795, GSE52093). Immune cell infiltration abundance was predicted using ImmuCellAI. GEO2R was used to select differentially expressed genes (DEGs), which were then processed for Gene Ontology (GO) and Kyoto Encyclopedia of Genes and Genomes (KEGG) pathway analyses. Additionally, hub genes linked to immune infiltration were found using functional and pathway enrichment, least absolute shrinkage and selection operator (LASSO), weighted gene co-expression network analysis (WGCNA), and differential expression analysis. Lastly, hub genes were validated and assessed using receiver operating characteristic (ROC) curves in the microarray dataset GSE52093. The hub gene expression and its connection to immune infiltration in TAAD were confirmed using both animal models and clinic data. **Results**: We identified the most important connections between macrophages, T helper cell 17 (Th17), iTreg cells, B cells, natural killer cells and TAAD. And screened seven hub genes associated with immune cell infiltration: *ABCG2*, *FAM20C*, *ELL2*, *MTHFD2*, *ANKRD6*, *GLRX*, and *CDCP1*. The diagnostic model in TAAD diagnosis with the area under ROC (AUC) was 0.996, and the sensitivity was 99.21%, the specificity was 98.67%, which demonstrated a surprisingly strong diagnostic power of TAAD in the validation datasets. The expression pattern of four hub DEGs (*ABCG2*, *FAM20C*, *MTHFD2*, *CDCP1*) in clinic samples and animal models matched bioinformatics analysis, and *ABCG2*, *FAM20C*, *MTHFD2* up-regulation, and the of *CDCP1* down-regulation were also linked to poor cardiovascular function. **Conclusions**: This study developed and verified an effective diagnostic model linked to immune infiltration in TAAD, providing new approaches to studying the potential pathogenesis of TAAD and discovering new medication intervention targets.

Keywords: type A aortic dissection; immune infiltration; immune cells; bioinformatics; diagnosis; differentially expressed genes

1. Introduction

A catastrophic cardiovascular emergency with a high mortality rate is aortic dissection (AD) [1,2]. A rupture in the intima frequently causes AD, which in turn causes blood to flow into the media layer of the aorta and the layers of the aortic wall to separate [3]. The aortic wall is being further eroded by this layer separation, which could lead to an aortic rupture or end-organ malperfusion. Depending on whether the ascending aorta is extended or not, AD was classified into kinds A (TAAD) and B (TBAD) according to the Stanford classification. Based on epidemiological research, the annual incidence of acute aortic dissection is estimated to be between 7 and 9 instances per 100,000 persons. This incidence is expected to grow by 5% year due to the rising prevalence of atherosclerosis and hypertension [4]. Because of the involvement of the cerebral or coronary arteries, sudden severe aortic regurgitation, and cardiac tamponade, TAAD is the most serious kind. Up to 90% of TAAD patients pass away within a year, and nearly half do so within a week [5]. On the other hand, TBAD has an acute fatality rate of about 10% [6,7]. The current recommendations for therapeutic approaches are medication for TBAD and emergency surgery for TAAD, taking into account the variations in fatality rates [8]. 15–30% mortality is still a high rate for TAAD, despite advances in treatment choices [9]. Thus, in order to create therapeutic options that work, it is imperative to comprehend the molecular pathophysiology of TAAD.

The primary pathological characteristic of AD is aortic medial degeneration [10]. Current research has demon-

strated that aortic medial degeneration and arterial wall remodeling, which occur prior to the initiation of aortic intima rupture [11], are associated with are associated with immunological and inflammatory-related pathways. Dissected aortic specimens contain active T and B lymphocytes as well as macrophages, especially along the ruptured media edge and the vasa vasorum [12]. One early-stage change in AD that promotes matrix degradation and angiogenesis is the activation of macrophages in the middle tunic membrane [13]. Still unknown, nevertheless, are the exact mechanisms that initiate immune cells' penetration of the aortic wall.

The development of sequencing technology encourages the use of bioinformatic analysis in health-related studies. A novel bioinformatics technique called weighted gene co-expression network analysis (WGCNA) can be used to find gene association modules and close the gap between gene expression and clinical characteristics [14]. WGCNA has recently been used extensively to search critical hub genes related to immune cell characteristics [15]. Based on a transcriptomic dataset, the recently developed ImmuCellAI algorithm calculates the infiltration abundance of 24 distinct immune cells groups [16]. The flow cytometry data is consistent with the validity of ImmuCellAI in determining the extent immune cell infiltration [17].

Here, we screened hub genes associated with immunological infiltrate cells using a systemic bioinformatics approach based on the Gene Expression Omnibus (GEO) database. Prior to applying WGCNA to define immune-related modules and selecting critical genes from these modules based on Pearson correlation coefficients (r) and the minor absolute shrinkage and selection operator (LASSO) algorithm, immune scores of each sample linked to TAAD were first determined using the ImmuCellAI algorithm. Additionally, an independent cohort, GSE52093, was used to develop and evaluate a binary logistic regression model based on crucial genes. This research offers a deeper understanding of the immunological regulatory systems that underlie the progression of TAAD.

2. Methods

2.1 Data Acquisition and Processing

The GEO database (https://www.ncbi.nlm.nih.gov/geo/) was consulted in order to obtain the DaExpression matrix of TAAD and associated clinical data. All of the data was collected up to January 31, 2024. The inclusion criteria: (I) samples in the dataset were obtained from the aorta; (II) the samples contained TAAD patients and Controls (patients without TAAD); (III) the dataset was based on human gene expression profiles. The inclusion criteria: samples without clinical information. Hereby, Ten TAAD tissues and ten normal Controls were included in the GSE153434 dataset [18], which was found on Illumina HiSeq X Ten Homo sapiens platform GPL20795. The R.DESeq2 package (version 1.30.1) was used to select differentially expressed genes (DEGs), with cutoffs of |log2 fold change (FC)| >1 and $p < 0.05$, and genes associated with differentially enriched immune cells were filtered by least absolute shrinkage and selection operator (LASSO). Volcano plots and heatmaps of DEGs were generated using the ggplot2 R package (Version R3.2.3) and heatmap R package (version R2.2.1) [19]. The RMA algorithm R.limma program was used to normalize data from five normal tissues and seven TAAD in the microarray dataset GSE52093, which acted as the external validation cohort [20].

2.2 Immune Infiltration Analyses

Immune cell infiltration and target gene expressions in TAAD was assessed using R (Version 3.6.3, The R Foundation for Statistical Computing, Vienna, Austria).

2.3 Construction of Gene Co-Expression Networks to Identify Critical Modules

Targeting the DEGs, a co-expression network was built with the R.WGCNA package (Version 4.1.3). The weighted adjacency matrix was constructed using a power function based on the soft threshold parameter β, and the scale-free network was ensured by setting $\beta = 18$ (scale-free $R^2 = 0.8$). In order to measure network connectivity, the adjacency matrix was transformed into a topological overlap matrix (TOM). Genes with similar expression profiles were then clustered based on TOM dissimilarity, and a gene dendrogram was used to divide the modules into minimum sizes of 50. After calculating the correlations between Pearson's module eigengenes (ME), modules with strong correlations were integrated at $r > 0.7$. Gene significance (GS) and module membership (MM) were used to identify the clinical trait-associated significant models. The immunophenotypic score of infiltrating immune cells was the clinical trait that was determined in this study.

2.4 Functional Enrichment Analysis

The R package clusterProfiler (Version 3.6.2) was utilized to perform enrichment studies for Kyoto Encyclopedia of Genes and Genomes (KEGG) and Gene Ontology (GO) in order to explore the possible pathways and functions of candidate hub genes in important modules. Cell components (CC), biological processes (BP), and molecular functions (MF) make up GO enrichment. It was decided to set statistical significances for only terms with false discovery rate (FDR) <0.05. The R packages ggplot2 and GO plot (Version 1.0.2) are used to display the enrichment findings.

2.5 Machine Learning

The Least Absolute Shrinkage and Selection Operator (LASSO) algorithm, a logistic regression method, was utilized to filter variables to improve the predictive performance in order to find the candidate biomarkers and create a diagnostic model for TAAD. The "glmnet" software package (Version 0.2.0) was used to screen the poten-

tial biomarkers. Next, to improve the accuracy, ensemble learning is employed to merge the Random Forest (RF) algorithm with numerous trees, and the Random Forest software package (Version 6.3.1) is utilized to reduce the pool of potential biomarkers. The hub genes for creating TAAD diagnostic models are the overlapping genes of the LASSO model and the MeanReduced Gini >2 genes of the RF model.

2.6 Hub-Gene Identification and Evaluation

Based on the clinical trait relevance and module connectivity, hub genes were selected from module genes using absolute value of GS >0.6 and MM >0.8 as thresholds. Next, we examined the connection between 24 immune cells and hub genes.

2.7 The Assessment of Diagnostic Marker Prediction Model

We evaluated the discriminatory power of the hub genes as TAAD biomarkers using the GSE52093 dataset, which included five normal samples and seven TAAD. Results were assessed using receiver operator characteristic (ROC) curves, where the area under the curve (AUC) was computed.

2.8 RealTime Quantitative PCR (RTqPCR)

Six clinical samples were obtained from Shaanxi Provincial People's Hospital; written informed consent forms were submitted by the patients or their families/legal guardians. The samples included three normal samples (Control group) from donors without TAAD and three TAAD samples (TAAD group) from patients with TAAD. Total RNA was extracted from aorta samples using the Total RNA Kit I (Omega Bio-tec, Inc., Norcross, GA, USA), then transformed into cDNA PrimeScript™ RT reagent kit (TaKaRa, Dalian, China). The Green PCR Master Mix System (Thermo Fisher Scientific, Waltham, MA, USA) was used in quantitative polymerase chain reaction (qPCR) using an ABI7500 Real-Time PCR System (Thermo Fisher Scientific). GAPDH served as the internal point of reference. The $2^{-\Delta\Delta CT}$ method was utilized to evaluate the relative fold change. Likewise, the aorta in the rat model is operated by the RT-qPCR experiment in the same manner as previously said. **Supplementary Table 1** contains a list of primer sequences that were employed.

2.9 Construction of Animal Models with TAAD

All animal experiments were in accordance with the guide for the care and use of laboratory animals established by United States National Institutes of Health (Bethesda, MD, USA). Male Sprague-Dawley (SD) rats, weighing between 90 and 120 grams, 4–6 weeks old, were obtained from the Laboratory Animal Center of the Medical Department of Xi'an Jiaotong University (Xi'an, China). The rats were randomly assigned to two groups: the Control group and the TAAD group. Each group contains six rats. Control group: Oral administration of 0.9% saline was given to the rats. For four weeks, once a day. TAAD group: For four weeks, rats were given 1 mg/kg/day of β-Aminopropionitrile (BAPN) dissolved in 0.9% saline orally. At the sixth week, tissue samples were collected, and all of the rats were put to death by breathing in an excessive amount of isoflurane. Prior to sacrifice, an echocardiogram was done, and the body weight was recorded during modeling.

2.10 Echocardiography

An intraperitoneal dose of 30 mg/kg pentobarbital was used to anesthetize the rats. Echocardiography was performed with ultra-high-resolution small animal ultrasound imaging system Vevo3100. Measurements were made of the ejection fraction (EF), fraction shortening (FS), aortic diameter (AO), and left coronary artery diameter (LCA). Three cardiac cycles' worth of data were analyzed to assess cardiovascular function.

2.11 Western Blotting

The whole protein was extracted from rat aortic tissue, separated using polyacrylamide gel electrophoresis containing sodium dodecyl sulfate, and then transferred onto nitrocellulose membranes (MilliporeSigma). The membranes were blocked for two hours at room temperature with 5% non-fat milk, and then incubated overnight at 4 °C, with the corresponding primary antibodies: Rabbit anti-Human ATP-binding cassette superfamily G menber 2 (ABCG2) (Dilution 1:1000, Abcam, Cambridge, UK), Rabbit anti-Rat ABCG2 (Dilution 1:1000, Abcam, Cambridge, UK), Rabbit anti-Human family with sequence similarity 20, member C (FAM20C) (Dilution 1:500, Abcam), Rabbit anti-Rat FAM20C (Dilution 1:500, Abcam), Rabbit anti-Human metabolism enzymemethylenetetrahydrofolate dehydrogenase 2 (MTHFD2) (Dilution 1:1000, Abcam), Rabbit anti-Rat MTHFD2 (Dilution 1:1000, Abcam), Rabbit anti-Human CUB domain containing protein 1 (CDCP1) (Dilution 1:1000, Abcam), Rabbit anti-Rat CDCP1 (Dilution 1:1000, Abcam), Rabbit anti-Human β-actin (Dilution 1:1000, Abcam), Rabbit anti-Rat β-actin (Dilution 1:1000, Abcam). The membranes were treated with the secondary antibody (Goat anti-Rabbit) for one hour at room temperature. Protein bands were visualized using an enhanced chemiluminescence (ECL) kit (Pierce, Thermo Fisher Scientific, Inc.).

2.12 Immunohistochemistry

Tissue sections fixed in paraffin, measuring 4 µm in thickness, were rehydrated and dewaxed. Antigen was extracted, then incubated respectively with the same monoclonal antibody as Western blotting at 4 °C overnight, then treated with Horseradish Peroxidase (HRP)-conjugated secondary antibody at room temperature for half an hour, fol-

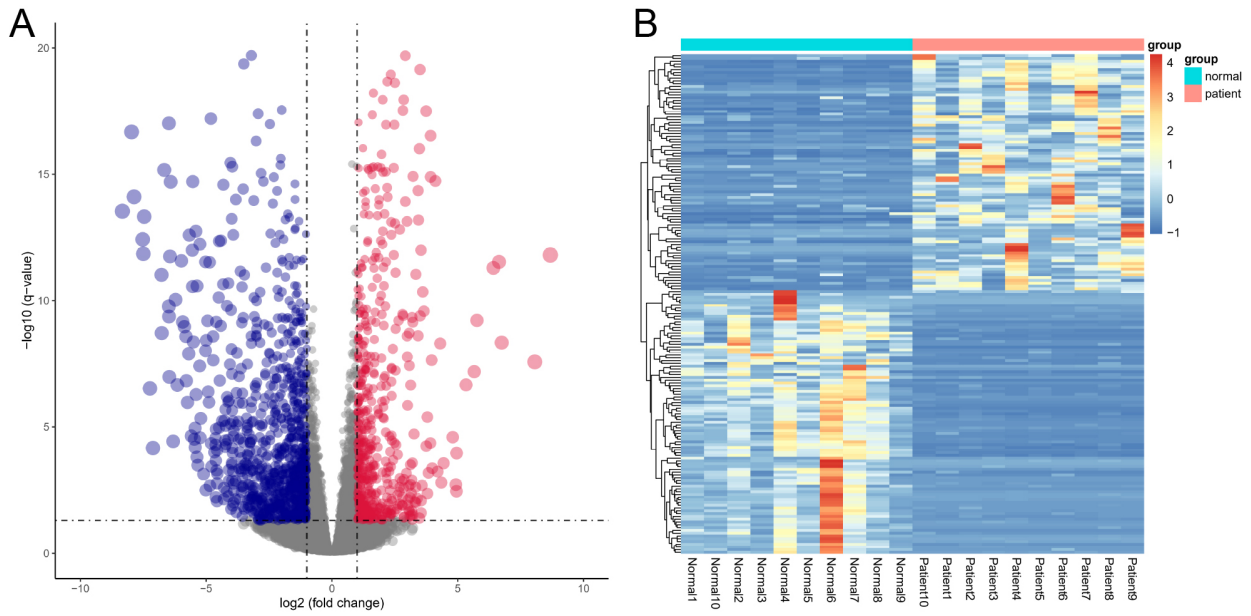

Fig. 1. Volcano plot (A) and heatmap (B) clustering for differentially expressed genes identified in type A aortic dissection (TAAD).

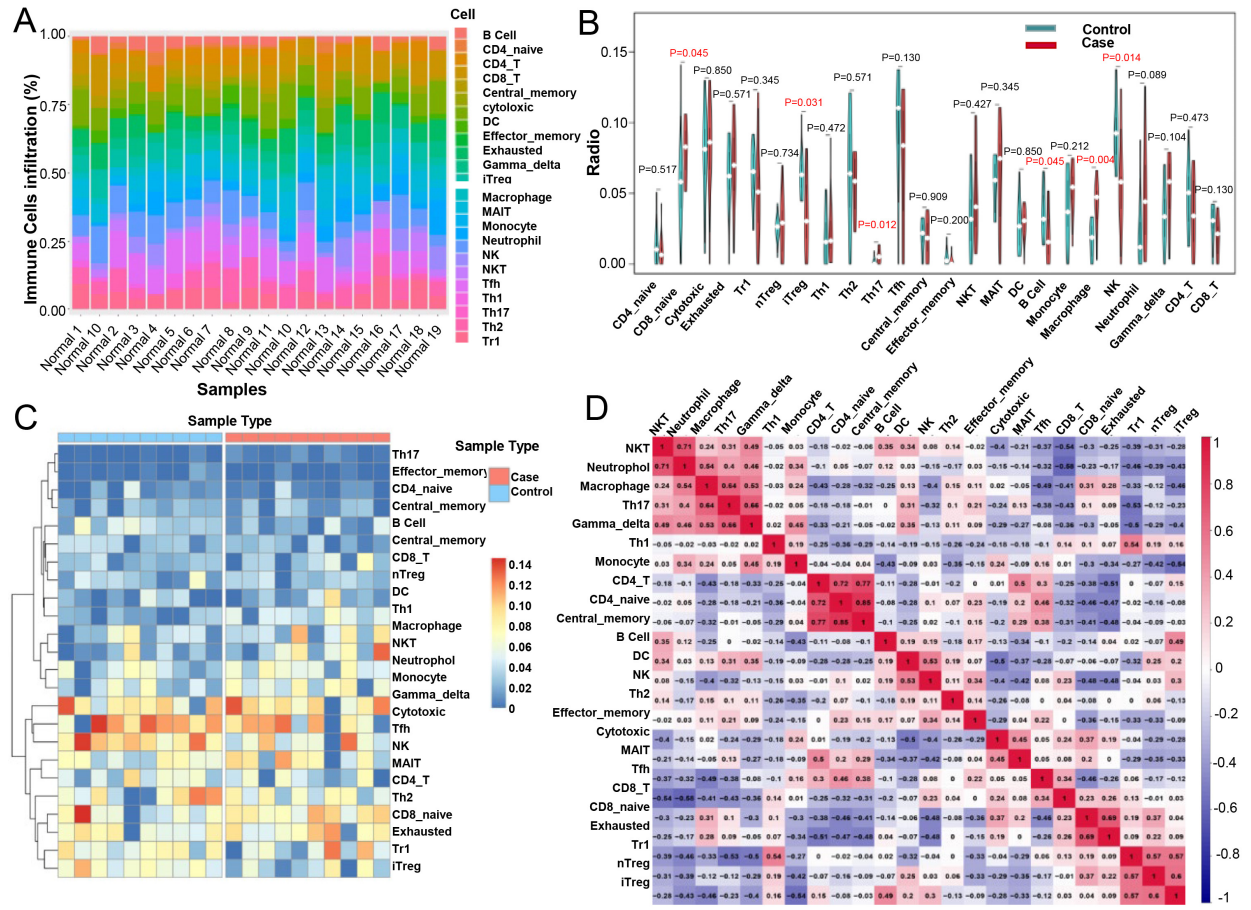

Fig. 2. The immunological cell infiltration landscape across all TAAD samples. (A) The violin plot displays the proportions of each immune cell. (B) The bar chart of immune cells. (C) The heatmap depicts the proportions of all 24 types of immune cells. (D) Correlations between the proportions of individual immune cells. Th17, T helper cell 17; DC, dendritic cells; NK, natural killer cells; MAIT, mucosal-associated invariant T.

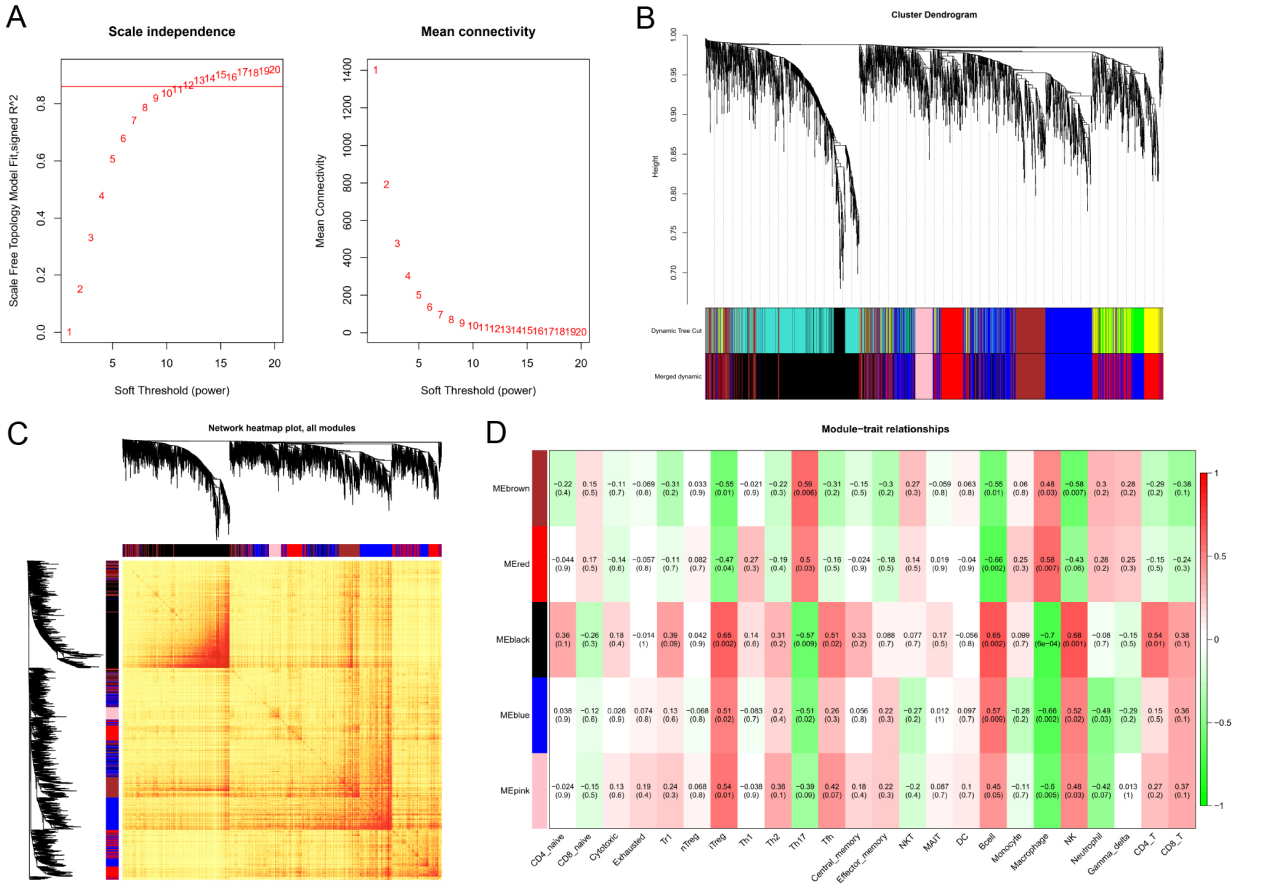

Fig. 3. Determination of key modules linked to immunophenotypic scores using weighted gene co-expression network analysis (WGCNA). (A) Selection of the soft-thresholding powers (β) based on the scale-free fit index and mean connectivity. (B) Hierarchical cluster analysis was adopted to identify co-expression modules. (C) The heatmap displayed selected module genes' topological overlap matrix (TOM). (D) The heatmap shows the correlations between modules and immune traits.

lowed by staining in DAB detection kit and restained with hematoxylin for 30 minutes. Ultimately, they were examined using a BX41 fluorescent microscope (Olympus Corporation, Tokyo, Japan), and visualized the immunoblot bands in a pre-cooled LAS4000 luminescent imager (GE, Boston, MA, USA).

2.13 Correlation between Hub Genes and Cardiovascular Parameters in Echocardiography

The Pearson algorithm was used to assess the parameter (EF%, FS%, and AO), and the R package "ggplot2" was used to illustrate the results [21].

2.14 Statistical Analysis

GraphPad Prism 8.0 (GraphPad Software, Inc., San Diego, CA, USA) was used to analyze all of the data, which were reported as the mean ± standard deviation (SD) of three separate experiments. Dunnett's post-hoc test was used after a one-way analysis of variance or Student's *t*-test to ascertain the statistical differences between the groups. Indicating a statistically significant difference was a p value less than 0.05.

3. Results

3.1 Identification of DEGs

1253 upregulated and 1486 downregulated DEGs were tested using the GSE153434 dataset. Fig. 1 illustrated the expression features of the DEGs in volcano plots (A) and heatmaps (B) for the ImmuCellAI, which indicated notable variations in the infiltrative abundance of 24 immune cells types between TAAD and normal samples. Among these, six cell types with significant differences were found in TAAD and the Control group, as shown in Fig. 2. More specifically, the TAAD group had higher concentrations of macrophages, T helper cell 17 (Th17), CD8 naive cells, dendritic cells (DC) and mucosal-associated invariant T (MAIT). By comparison, the Control group showed a significant enrichment of natural killer cells (NK), induced regulatory T cells (iTregs), and B cells (Fig. 2A–C). Moreover, macrophages showed the strongest negative correlation with iTregs cells and the strongest positive correlation with Th17 cells, according to the correlation matrix data (Fig. 2D).

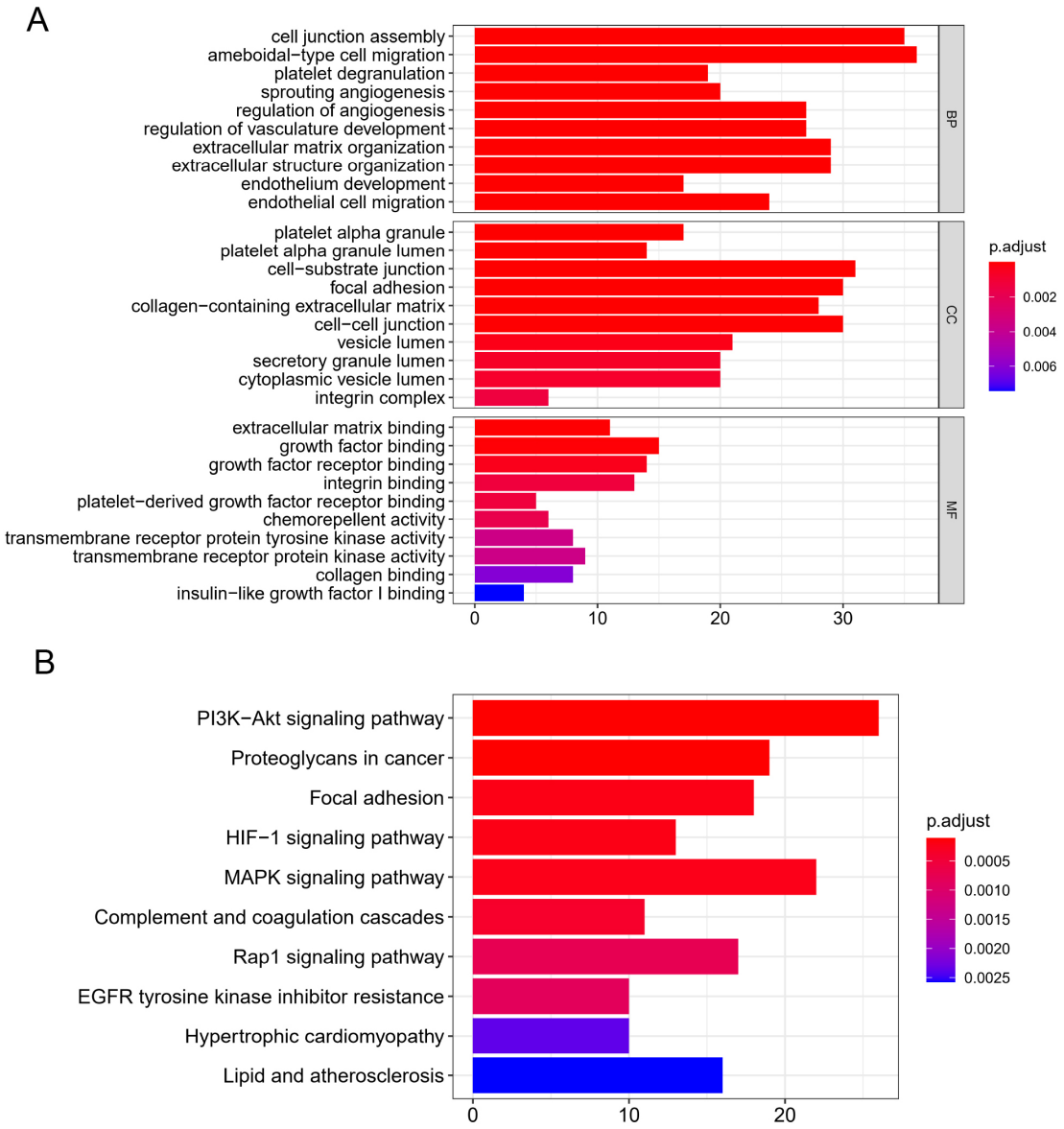

Fig. 4. Gene Ontology (GO) functions (A) and Kyoto Encyclopedia of Genes and Genomes (KEGG) pathways (B) enrichment analyses of candidate genes.

3.2 Identification of Key Modules by WGCNA

The WGCNA network was built from these DEGs. Based on the scale-free topology model and average connectivity, the gene regulation network's ideal soft threshold power is 12 (Fig. 3A). The hierarchical clustering tree was structured using dynamic hybrid cutting to create five modules (brown, red, blue, black, and pink) (Fig. 3B,C). The network heat map was plotted based on the five modules and 24 immune cell types (Fig. 3D). The module-trait relationships revealed that all five modules were linked to macrophages and iTreg, while four modules (brown, red, blue, and black) were linked to Th17 cells, four modules with NK cells, and none with CD8 naive cells. Based on MM >0.8 and GS >0.6 standards, 432 genes in all modules were chosen as hub genes for further analysis.

3.3 Enrichment Analyses and Mechanism Explorations

GO and KEGG enrichment analyses were carried out to identify 432 genes' putative activities and pathways. Consequently, 461 associated BPs and 22 KEGG pathways with statistical significance were found. Cell junction assembly, cell migration, platelet degranulation, angiogenesis, and vascular development were found to be enriched in BP, according to GO analysis. Additionally, we found that CC was associated with an enrichment of platelet alpha granules, cell-cell junctions, focal adhesion, and cell-substrate junctions. Furthermore, MF was discovered to have an enrichment of extracellular matrix binding, growth factor binding, integrin binding, and chemorepellent activity (Fig. 4A). More significantly, the KEGG data showed that the hub genes had a higher probability of enrichment

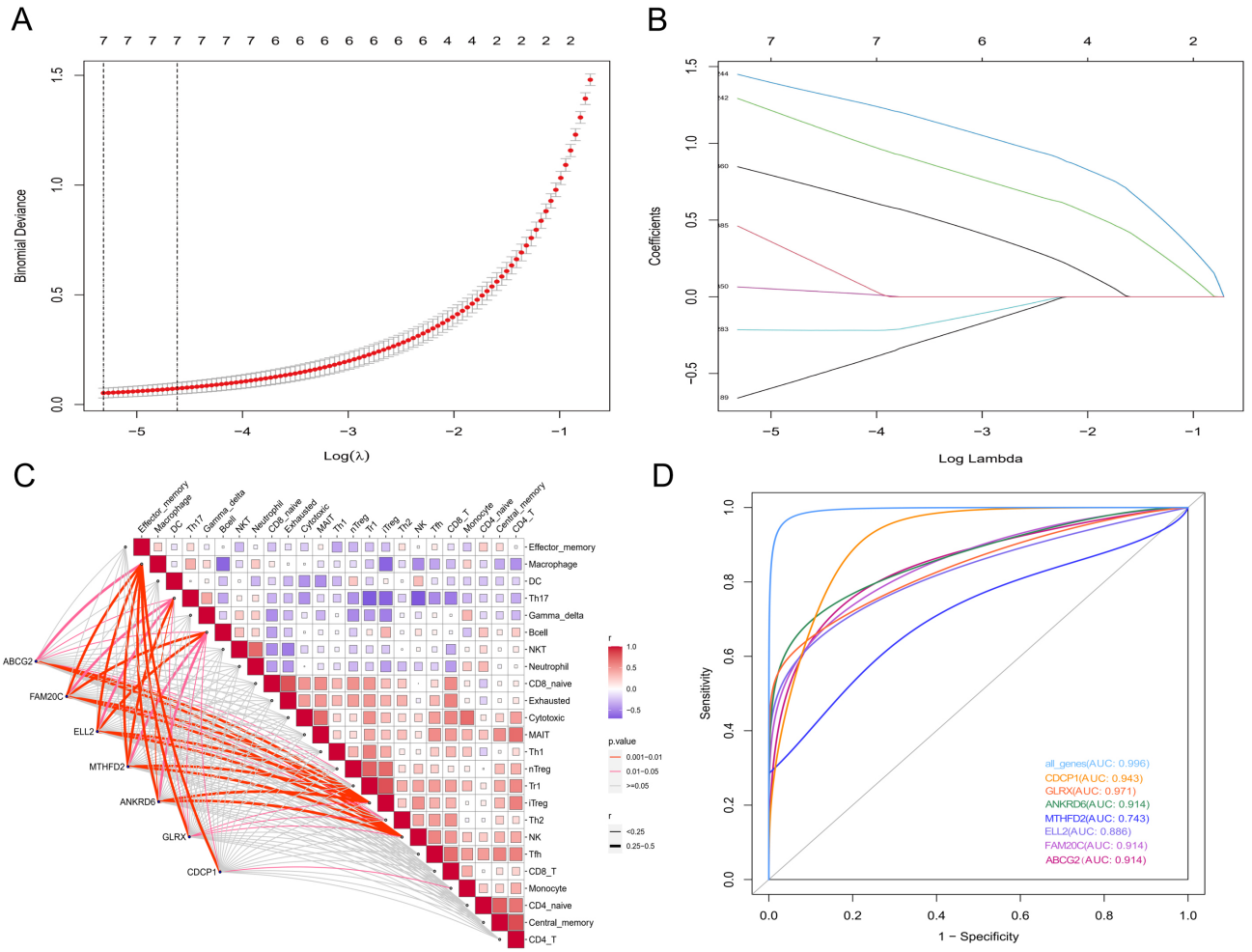

Fig. 5. Identification and verification of hub-genes. (A) The coefficient profile plot is generated based on the log (lambda) sequence. (B) Least absolute shrinkage and selection operator (LASSO) coefficients for seven hub genes. (C) Correlation between hub genes and 24 types of immune cells. (D) External validation of the diagnostic potential of each hub gene based on the GSE52093 dataset. AUC, the area under receiver operating characteristic.

in terms of PI3K-Akt signaling pathway, HIF-1 signaling pathway, lipid and atherosclerosis (Fig. 4B).

3.4 Identification and Verification of Hub-Genes

Seven genes—*ABCG2*, *FAM20C*, *ELL2*, *MTHFD2*, *ANKRD6*, *GLRX*, and *CDCP1*—among the candidate 432 genes were found to be hub genes and potential immune-related diagnostic biomarkers of TAAD using the LASSO algorithm (Fig. 5A,B). Seven hub genes were shown to be strongly correlated with macrophages, Th17, B cells, iTregs, and natural killer cells (Fig. 5C). Immune cells were also found to differ significantly in TAAD. Using the GSE52093 dataset, the discriminating ability of all seven genes was further confirmed. Then the seven optimal genes were used to construct the diagnostic model. The diagnostic model in TAAD diagnosis with the area under ROC (AUC) was 0.996, and the sensitivity was 99.21%, the specificity was 98.67%. The ROC curve analysis demonstrated a strong discriminatory ability for TAAD (Fig. 5D), indicating that all seven genes could serve as potential biomarkers and are implicated in inflammation and immune cell infiltration in TAAD.

3.5 The Validation of the Relationship between Hub Genes and TAAD in Clinical Samples

Three hub genes (*ABCG2*, *FAM20C*, *MTHFD2*) had significantly higher mRNA expression levels in the TAAD group compared to the Control group ($p < 0.05$), according to RT-qPCR data. Nevertheless, there was a significant downregulation of one hub gene (*CDCP1*) in the TAAD group ($p < 0.05$). The two groups' changes were particularly pronounced in *ABCG2*, *FAM20C*, *MTHFD2*, and *CDCP1* (Fig. 6A). Thus, in the tests that followed, we concentrated on confirming the connection between these four hub genes and TAAD. By using Western blotting and immunohistochemistry, we were able to further elucidate the differences in the protein expression levels of ABCG2, FAM20C, MTHFD2, and CDCP1 between the Control

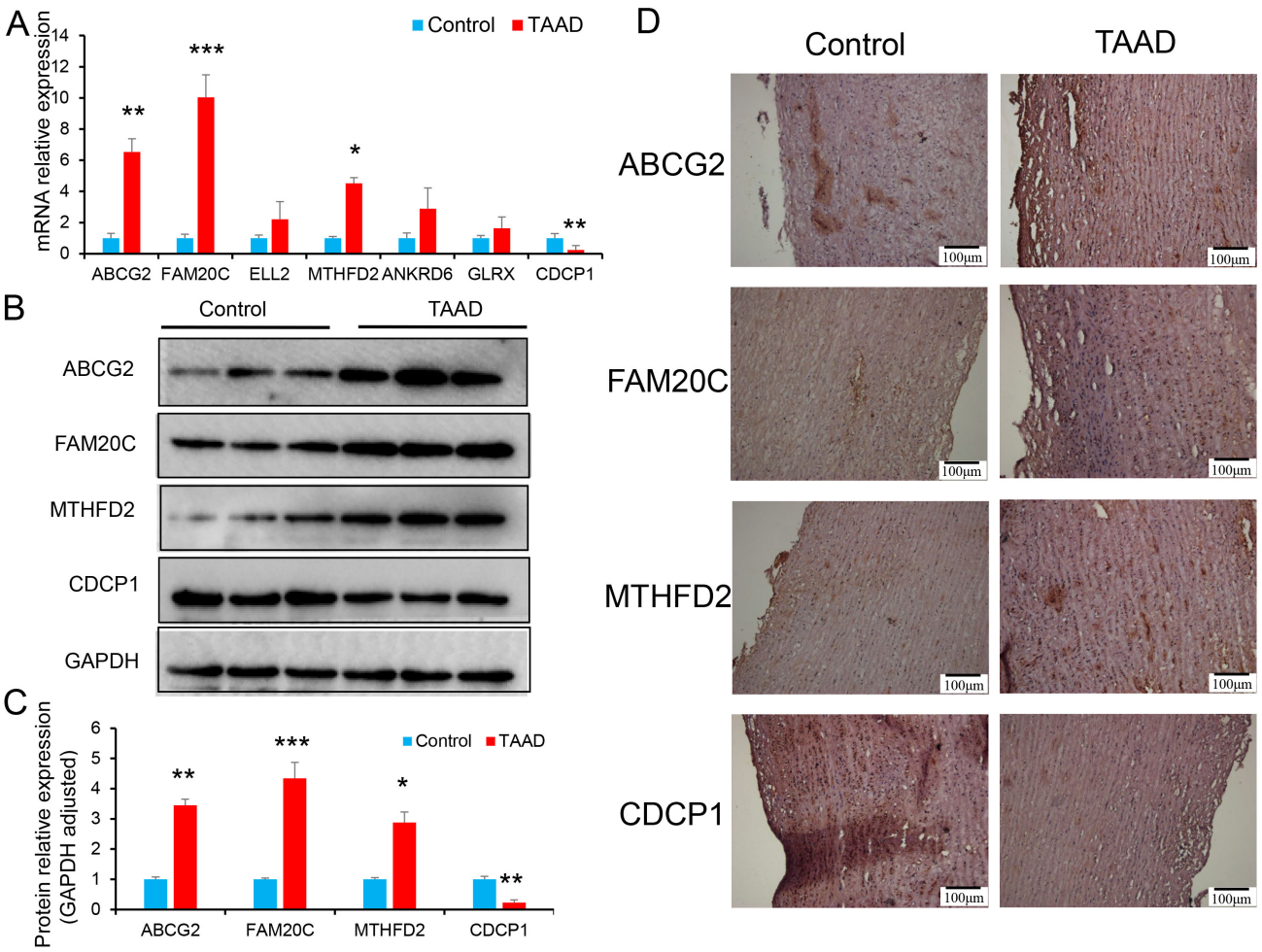

Fig. 6. The relationship between hub genes and TAAD in clinical samples is validated. (A) The mRNA level of seven hub genes in the Control and TAAD groups. (B,C) Western blotting and quantitative analysis display ABCG2, FAM20C, MTHFD2, and CDCP1 protein levels in aortic tissues. (D) Immunohistochemistry analysis displaying ABCG2, FAM20C, MTHFD2, and CDCP1 protein levels in aortic tissues. Scale bars = 100 μm. Compared with the Control group, *$p < 0.05$, **$p < 0.01$, ***$p < 0.001$.

and TAAD groups. Western blotting results indicated that CDCP1 was lowered ($p < 0.05$), whereas the levels of protein expression of ABCG2, FAM20C, and MTHFD2 (Fig. 6B,C). The results of immunohistochemistry were consistent with those of the Western blot (Fig. 6D).

3.6 Experimental Verification of the Correlation between Four Central Genes and TAAD

We created TAAD rat models with β-Aminopropionitrile to confirm the link between these four hub genes and TAAD. During modeling, the TAAD group had considerably lower body weight than the Control group ($p < 0.05$) (Fig. 7A). qPCR analysis of aorta samples revealed higher mRNA expression levels for *ABCG2*, *FAM20C*, and *MTHFD2* ($p < 0.05$) and decreased CDCP1 ($p < 0.05$) in the TAAD group compared to the Control group (Fig. 7B). Compared to the Control group, the TAAD group had significantly lower EF% and FS% ($p < 0.001$) and higher AO ($p < 0.001$). LCA was increased in the TAAD group, although not significantly compared to the Control group (Fig. 7C,D). We further analyzed the correlation between four hub genes (*ABCG2*, *FAM20C*, *MTHFD2*, and *CDCP1*) and cardiac function in the TAAD group. The results showed the number of PCR cycles of *ABCG2*, *FAM20C*, *MTHFD2* and *CDCP1* both had significant positive correlations with EF%, FS% and AO ($p < 0.001$) (Fig. 7E). In summary, the upregulation of *ABCG2*, *FAM20C*, and *MTHFD2* and the downregulation of CDCP1 in aorta tissues were closely linked to cardiac and vascular function decline.

3.7 Protein Expression Levels of Four Hub Genes in TAAD Rats

The Western blotting results indicated that the protein expression levels of ABCG2, FAM20C, and MTHFD2 were increased, and CDCP1 was decreased in the TAAD group compared to the Control group. The findings were in line with the results obtained from mRNA analysis, with

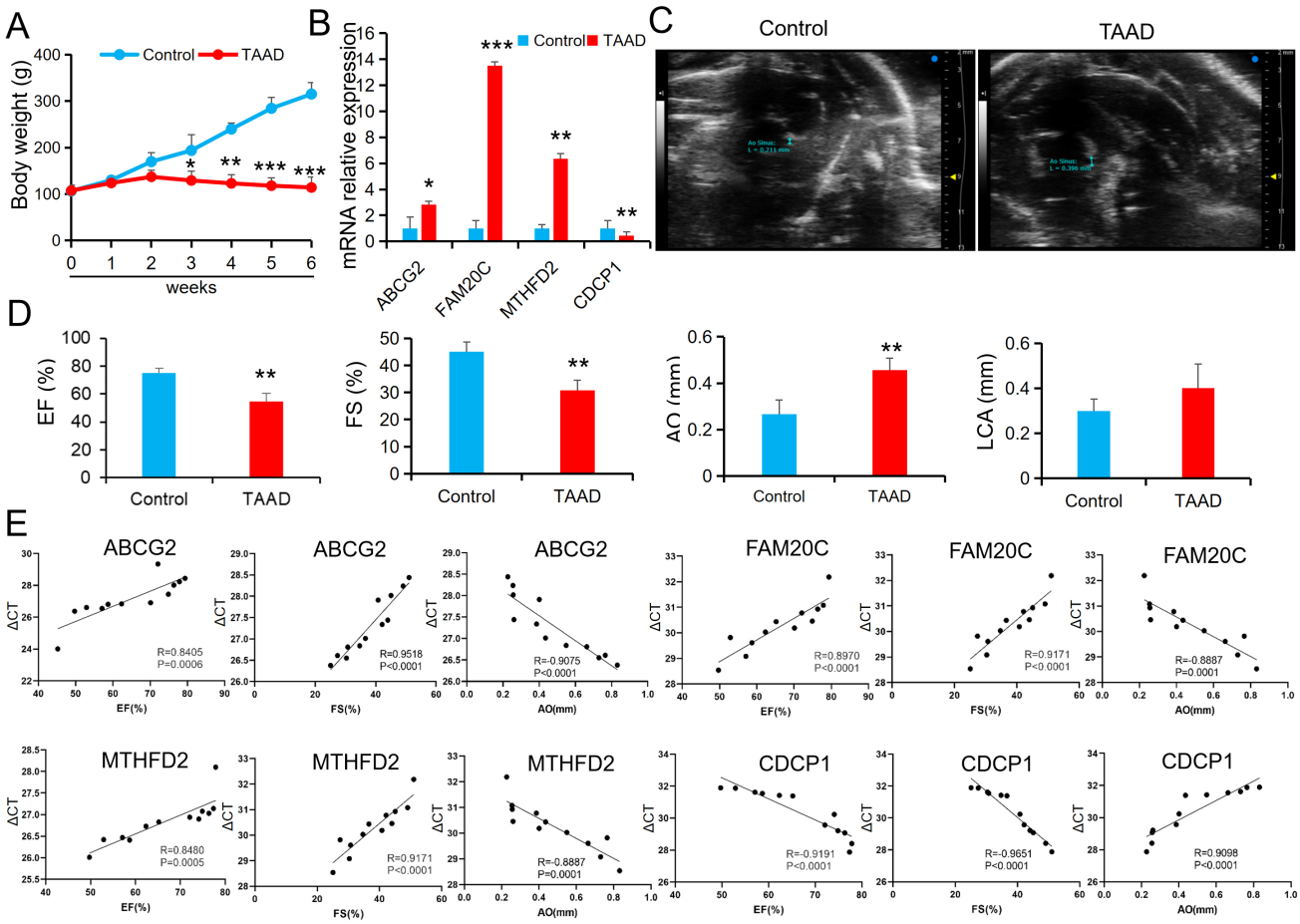

Fig. 7. The relationship between *ABCG2*, *FAM20C*, *MTHFD2*, *CDCP1* mRNA levels, and TAAD in rats model. (A) The body weight in the Control and TAAD group. (B) *ABCG2*, *FAM20C*, *MTHFD2*, *CDCP1* mRNA levels in the Control and TAAD group. (C) The echocardiography features in the Control and TAAD groups. (D) The correlations between four optimal hub genes *ABCG2*, *FAM20C*, *MTHFD2*, *CDCP1* mRNA levels, and coronary artery functional parameters in the Control and TAAD group. (E) Correlation analysis between four hub genes and cardiovascular function. Compared with the Control group, $*p < 0.05$, $**p < 0.01$, $***p < 0.001$.

a statistical significance of $p < 0.05$ (Fig. 8A,B). The immunohistochemistry results revealed an irregular arrangement of endothelial cells in the vascular intima, partial damage to the intima, and an increase in the thickness of the vascular media. Additionally, the protein expression levels of ABCG2, FAM20C, MTHFD2, and CDCP1 were found to be in agreement with those observed in western blotting (Fig. 8C).

4. Discussion

The ImmuCellAI algorithm was employed in this study to ascertaine the immune cell composition of TAAD. Moreover, five immune-related modules and 432 candidate hub genes were discovered by WGCNA. Function and KEGG pathway enrichment analyses provided insights into the putative TAAD hub genes' processes. Seven hub genes, *ABCG2*, *FAM20C*, *ELL2*, *MTHFD2*, *ANKRD6*, *GLRX*, and *CDCP1*, were screened as immune-related hub genes using LASSO regression. These hub genes and immune cell infiltration associated with TAAD were found to be significantly correlated, according to correlation analysis. Our findings demonstrated TAAD's strong diagnostic potential in the validation datasets, suggesting that these genes could serve as prospective biomarkers and have a role in immune cell infiltration associated with TAAD.

AD has a complex etiology and mechanism. It was initially believed that AD began with an aortic intima rupture [22]. High-pressure blood flow from the damaged intima divides the aortic media from the adventitia. But according to a new theory, AD may begin with media inflammation. The aortic medium may be chronically irritated prior to the onset of AD. The intima finally bursts and results in AD when there is continuous high-pressure blood flow [23].

Chen *et al.* [24] reported that the infiltration of inflammatory cells, such as macrophages, neutrophils, and T lymphocytes, increases with the progression of the disease. Here, we employed the ImmuCellAI algorithm to obtain insight into the immunological milieu by computing infiltration abundances of 24 immune cells based on high-throughput sequencing data of TAAD tissue samples. The

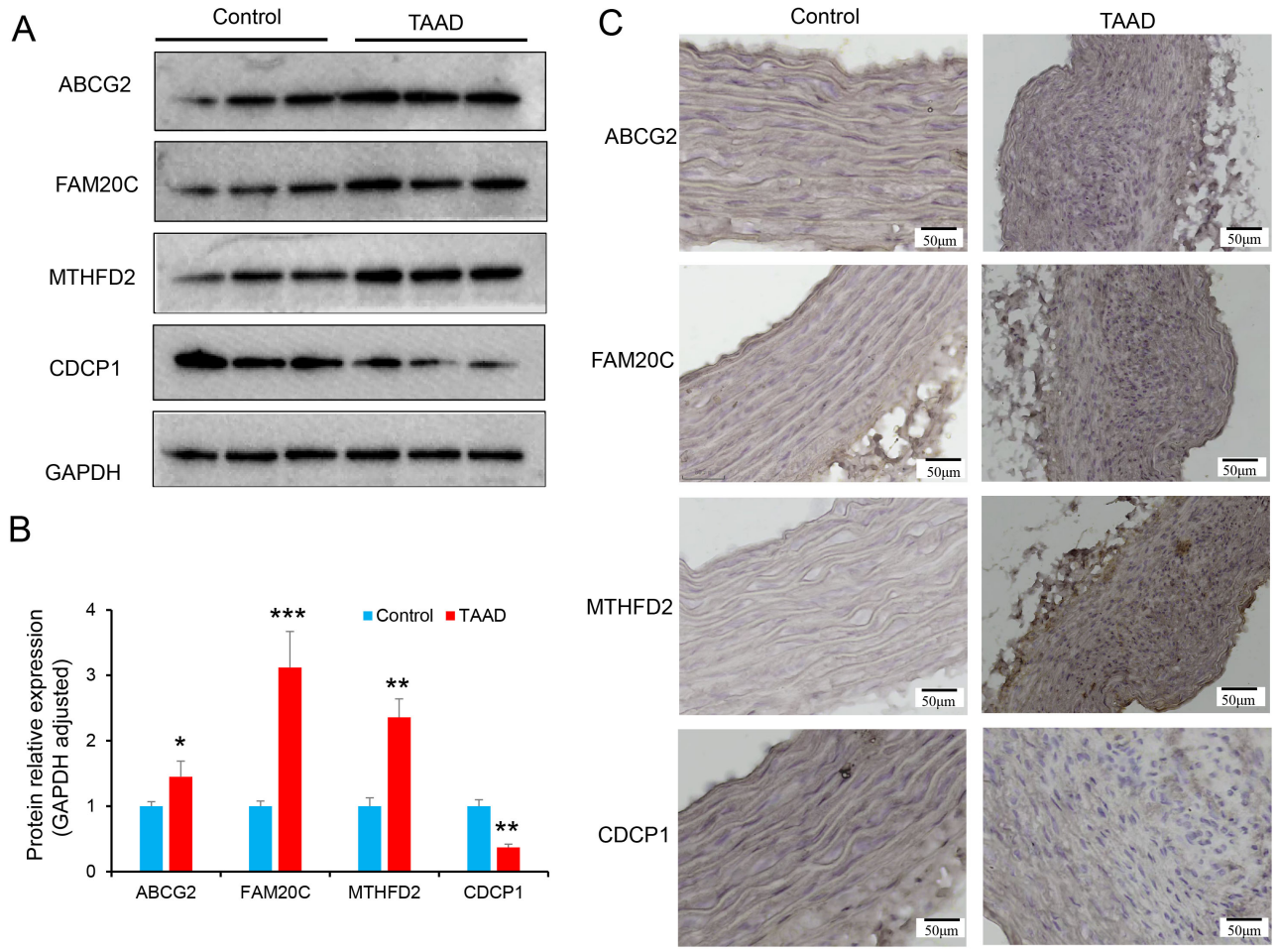

Fig. 8. The relationship between ABCG2, FAM20C, MTHFD2, CDCP1 protein levels, and TAAD in rats model. (A,B) Protein levels of ABCG2, FAM20C, MTHFD2, and CDCP1 by western blotting and quantitative analysis in aortic tissues in Control and TAAD groups. (C) Immunostaining of ABCG2, FAM20C, MTHFD2, CDCP1 protein expression. Scale bars = 50 μm. Compared with Control group, $*p < 0.05$, $**p < 0.01$, $***p < 0.001$.

TAAD group exhibited a higher macrophage score following the previous findings [25].

According to a number of studies, macrophages initially enter the aortic media and adventitia, where they trigger a local inflammatory response that causes neutrophils and T cells from various places to congregate in the aorta [26]. Targeting the reduction of mononuclear/macrophage was shown by Li *et al.* [27] to dramatically prevent AD development as well as T lymphocyte and neutrophil infiltrations. The majority of immunological responses are produced by T cells, various subtypes of which have distinct functions in the inflammatory event of TAAD [28]. Consistent with studies from peripheral blood [29], our results indicated a higher proportion of Th17 but a lower infiltration of Tregs in the TAAD group. An imbalance in Th17/Treg cells is considered to be a potential cause of atherosclerosis and plaque rupture in TAAD. Furthermore, B lymphocytes might possibly be involved in the formation of TAAD [30]. In line with the current findings, a number of thorough bioinformatic investigations have recently verified the distinction in immune infiltrates between AD and normal people [31,32]. Consequently, our findings showed that immune cell infiltration played a role in the pathophysiology of AD and could inspire new treatment strategies to stop the aortic disease's advancement.

Our research identified seven hub genes that were correlated with immune cell infiltrations at the expression level, indicating a potential role for these genes in facilitating the progression of TAAD. A family member of the ATP-binding cassette (ABC) transporter, ATP-binding cassette subfamily G member 2 (ABCG2) is the molecular cause of multidrug resistance in a variety of cancer cells [33]. ABCG2 has been recently demonstrated to be expressed in numerous normal tissues and may contribute to tissue defense by regulating redox and inflammation in a variety of diseases [34]. ABCG2$^{-/-}$ mice exhibited a more substantial macrophage infiltration than WT mice, as demonstrated by Sarkadi *et al.* [35]. The study has linked ABCG2 to

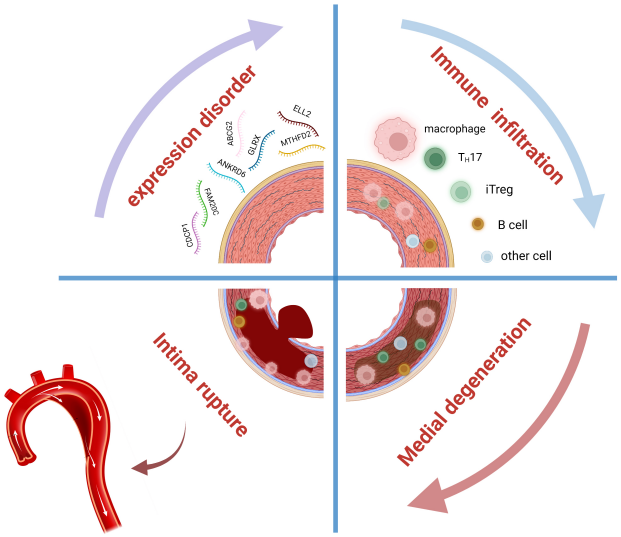

Fig. 9. The proposed mechanism for the formation of Stanford TAAD was drawed by Figdraw software. First, the environmental or genetic factors lead to aberrant hub gene expression, such as *ABCG2*, *FAM20C*, *ELL2*, *MTHFD2*, *ANKRD6*, *GLRX*, and *CDCP1*. Second, despite the lack of histological alterations, the aberrant gene expression causes several immune cell subtypes to infiltrate, such as Th17, iTreg cells and macrophage. Third, aortic medial degeneration is caused by immune cell infiltration and persistent chronic inflammation. Last, under continuous high-pressure blood flow, the aortic intima tears, causing the aorta's layers to separate.

T-cell differentiation [36]. We found that ABCG2 mRNA and protein were considerably enhanced in TAAD, although more research is needed to validate its role in T-cell differentiation. BP involves a Golgi casein kinase, FAM20C, which phosphorylates many secreted proteins and interacts with many substrates [37]. Bioinformatics showed that FAM20C is harmful to pan-cancer and positively correlates with T cells, macrophages, neutrophils, and dendritic cells [38]. High plasma cell expression of the transcription elongation factor elongation factor for RNA polymerase II 2 (ELL2) governs B lymphocyte proliferation and IgA production [39]. The knockout of ELL2 resulted in a weakened humoral immune response in mice and decreased the number and morphological changes of plasma cells [40]. Multiple myeloma studies linked ELL2 mutations to total IgA [41]. MTHFD2 regulates purine synthesis and signal transmission to increase activated T cell proliferation and inflammatory cytokines [42]. Recent research shows that MTHFD2 prevents FoxP3 upregulation from influencing Treg cell development [43]. Ankyrin repeat domain 6 (ANKRD6), a ubiquitous protein involved in early human development, regulates critical protein interactions and promotes cell proliferation and invasion via the Jun N-terminal kinase (JNK) pathway. According to Bai *et al.* [44], ANKRD6 may impact the immunological milieu by affecting the WNT pathway, which recruits and regulates colon cancer-infiltrating immune cells. Glutaredoxin-1 (GLRX) is an essential thioltransferase that modulates gene transcription and redox signaling regulated by the protein S-glutathionylation [45,46]. GLRX activates macrophages to enhance glioma growth, demonstrating its importance in the immunological response [47]. Single-pass transmembrane CDCP1 interacts with cell-cell or cell-extracellular matrix [48]. CDCP1 regulates tumor cell survival and metastasis [49], but a new study suggests it may also modulate the immune system [50]. Interestingly, all seven hub genes were strongly associated with macrophage infiltration, and most were closely associated with Th17 or iTreg infiltration. Additionally, all seven hub genes had robust diagnostic capacities for TAAD. Thus, immunological modulation may contribute to TAAD development. Our clinic samples and animal model experiment results demonstrated an expression pattern compatible with bioinformatics analysis for four hub DEGs (*ABCG2*, *FAM20C*, *MTHFD2*, *CDCP1*). ABCG2, FAM20C, MTHFD2, and CDCP1 upregulation and CDCP1 downregulation were also linked to poor cardiovascular function. Future research is needed to confirm the role of integrated gene regulation in immune response.

Previous research has used bioinformatics analysis based on the GEO database to examine hub genes linked to immune infiltration and AD progression [51,52]. Nevertheless, there is no overlap between the hub genes listed here and those that have already been found. The current study differs from earlier research in a number of ways, including:

(1) To determine the makeup of immune cell composition, we used ImmuCellAI analysis. ImmuCellAI algorithm outperforms other algorithms, such as CIBERSORT, xCell, and TIMER, according to the flow cytometry results [16].

(2) The significant thing about this work is that ImmuCellAI verified the link between immune infiltrating cells and crucial genes expression. WGCNA was used to identify modules associated with resistant cell-related. Further use of LASSO was made to eliminate duplication and screen hub genes, ensuring a strong correlation between immune cell infiltration and critical genes.

(3) We established a strong correlation between decreased cardiovascular function, which leads to TAAD, and the up-regulation of ABCG2, FAM20C, and MTHFD2 and the down-regulation of CDCP1.

However, this study has a number of shortcomings. Initially, bioinformatics analysis using data from public database sources produced findings that need to be thoroughly assessed and validated in the subsequent research. Second, the causal relationship between hub genes and immune cell infiltration could not be established by immune infiltration analysis based on transcriptome data. Therefore, more investigation is required to clarify the possible pathways.

5. Conclusions

In conclusion, this work innovatively combined LASSO logistic regression, ImmuCellAI, and WGCNA algorithms to screen immune infiltration-related hub genes in TAAD. We found that seven hub genes, *ABCG2*, *FAM20C*, *ELL2*, *MTHFD2*, *ANKRD6*, *GLRX*, and *CDCP1*, were strongly linked to the invasion of macrophage and Th17 or iTreg infiltration. Then, by triggering the internal immune response, we may accelerate the development of TAAD by establishing and validating an efficient diagnostic model linked to the hub genes in TAAD (Fig. 9). These findings provide new insight into the pathogenesis of TAAD and identify new targets for immunotherapy and disease prevention.

Availability of Data and Materials

The original data presented in the study are included in the article/Supplementary material, which will be made available by the corresponding author.

Author Contributions

XH and CX were responsible for designing the overall study, processing bioinformatic analysis, and writing the manuscript. GZ recruited the patient samples and collected the clinical data. YF, XZ, YL and JS were responsible for processing experimental validation. FL and YD were accountable for analyzing and interpreting the data. All authors viewed and approved the final manuscript for publication. All authors contributed to editorial changes in the manuscript. All authors have participated sufficiently in the work and agreed to be accountable for all aspects of the work.

Ethics Approval and Consent to Participate

Human samples protocols obtained approval from the Ethics Committee of Shaanxi Provincial People's Hospital (No: SPPH-LLBG-17-3.2), and adhered strictly to the Declaration of Helsinki (seventh revision, 2013). A written consent was signed by the patients or their families/legal guardians. All animal use procedures and ethics were reviewed and approved by the Biomedical Ethics Committee of Health Science Center of Xi'an Jiaotong University (No. XJTUAE2023-110). All animal experiments were in accordance with the guide for the care and use of laboratory animals established by United States National Institutes of Health (Bethesda, MD, USA).

Acknowledgment

Not applicable.

Funding

This work was supported by International Science and Technology Cooperation Program Project of Key Research and Development Plan of Shaanxi Province (2020KWZ-20), Shaanxi Province Innovation Capability Support Plan (2024RS-CXTD-84), the Science and Technology Program of Xi'an (23YXYJ0186), and the Basic Natural Science Foundation of Shaanxi Province (2024JC-YBMS-654), the Key Projects of Shaanxi Provincial Department of Education (22JS035).

Conflict of Interest

The authors declare no conflict of interest.

Supplementary Material

Supplementary material associated with this article can be found, in the online version, at https://doi.org/10.31083/j.fbl2909318.

References

[1] Carrel T, Sundt TM, 3rd, von Kodolitsch Y, Czerny M. Acute aortic dissection. Lancet. 2023; 401: 773–788.

[2] Rylski B, Schilling O, Czerny M. Acute aortic dissection: evidence, uncertainties, and future therapies. European Heart Journal. 2023; 44: 813–821.

[3] Yang X, Xu C, Yao F, Ding Q, Liu H, Luo C, *et al*. Targeting endothelial tight junctions to predict and protect thoracic aortic aneurysm and dissection. European Heart Journal. 2023; 44: 1248–1261.

[4] Parve S, Ziganshin BA, Elefteriades JA. Overview of the current knowledge on etiology, natural history and treatment of aortic dissection. The Journal of Cardiovascular Surgery. 2017; 58: 238–251.

[5] Chandiramani A, Al-Tawil M, Rajasekar T, Elleithy A, Kakar S, Haneya A, *et al*. Incidence Rates of Penn Classes and Class-Specific Mortality in Acute Type A Aortic Dissection Patients: An Epidemiologic Systematic Review and Meta-Analysis. Journal of Cardiothoracic and Vascular Anesthesia. 2024; 38: 1558–1568.

[6] Barton M, Wang H. An Uncommon Presentation of Acute Thoracic Aortic Dissection. Journal of Clinical Medicine Research. 2023; 15: 332–335.

[7] Meccanici F, Gökalp AL, Thijssen CGE, Mokhles MM, Bekkers JA, van Kimmenade R, *et al*. Male-female differences in acute thoracic aortic dissection: a systematic review and meta-analysis. Interactive Cardiovascular and Thoracic Surgery. 2022; 34: 616–627.

[8] Harris KM, Nienaber CA, Peterson MD, Woznicki EM, Braverman AC, Trimarchi S, *et al*. Early Mortality in Type A Acute Aortic Dissection: Insights From the International Registry of Acute Aortic Dissection. JAMA Cardiology. 2022; 7: 1009–1015.

[9] Evangelista A, Isselbacher EM, Bossone E, Gleason TG, Eusanio MD, Sechtem U, *et al*. Insights From the International Registry of Acute Aortic Dissection: A 20-Year Experience of Collaborative Clinical Research. Circulation. 2018; 137: 1846–1860.

[10] Cifani N, Proietta M, Tritapepe L, Di Gioia C, Ferri L, Taurino M, *et al*. Stanford-A acute aortic dissection, inflammation, and metalloproteinases: a review. Annals of Medicine. 2015; 47: 441–446.

[11] Yin ZQ, Han H, Yan X, Zheng QJ. Research Progress on the Pathogenesis of Aortic Dissection. Current Problems in Cardiology. 2023; 48: 101249.

[12] Zhao HL, Tang ZW, Diao YF, Xu XF, Qian SC, Li HY, *et al*. Inflammatory profiles define phenotypes with clinical relevance in

acute type A aortic dissection. Journal of Cardiovascular Translational Research. 2023; 16: 1383–1391.
[13] del Porto F, Proietta M, Tritapepe L, Miraldi F, Koverech A, Cardelli P, *et al*. Inflammation and immune response in acute aortic dissection. Annals of Medicine. 2010; 42: 622–629.
[14] Langfelder P, Horvath S. WGCNA: an R package for weighted correlation network analysis. BMC Bioinformatics. 2008; 9: 559.
[15] Xia MD, Yu RR, Chen DM. Identification of Hub Biomarkers and Immune-Related Pathways Participating in the Progression of Antineutrophil Cytoplasmic Antibody-Associated Glomerulonephritis. Frontiers in Immunology. 2022; 12: 809325.
[16] Miao YR, Zhang Q, Lei Q, Luo M, Xie GY, Wang H, *et al*. ImmuCellAI: A Unique Method for Comprehensive T-Cell Subsets Abundance Prediction and its Application in Cancer Immunotherapy. Advanced Science. 2020; 7: 1902880.
[17] Guo J, Tong C, Shi J, Li X, Chen X. A prognosis model for predicting immunotherapy response of esophageal cancer based on oxidative stress-related signatures. Oncology Research. 2023; 32: 199–212.
[18] Zhou Z, Liu Y, Zhu X, Tang X, Wang Y, Wang J, *et al*. Exaggerated Autophagy in Stanford Type A Aortic Dissection: A Transcriptome Pilot Analysis of Human Ascending Aortic Tissues. Genes. 2020; 11: 1187.
[19] Love MI, Huber W, Anders S. Moderated estimation of fold change and dispersion for RNA-seq data with DESeq2. Genome Biology. 2014; 15: 550.
[20] Ritchie ME, Phipson B, Wu D, Hu Y, Law CW, Shi W, *et al*. limma powers differential expression analyses for RNA-sequencing and microarray studies. Nucleic Acids Research. 2015; 43: e47.
[21] Gustavsson EK, Zhang D, Reynolds RH, Garcia-Ruiz S, Ryten M. ggtranscript: an R package for the visualization and interpretation of transcript isoforms using ggplot2. Bioinformatics. 2022; 38: 3844–3846.
[22] Luo Y, Luo J, An P, Zhao Y, Zhao W, Fang Z, *et al*. The activator protein-1 complex governs a vascular degenerative transcriptional programme in smooth muscle cells to trigger aortic dissection and rupture. European Heart Journal. 2024; 45: 287–305.
[23] Tao Y, Li G, Yang Y, Wang Z, Wang S, Li X, *et al*. Epigenomics in aortic dissection: From mechanism to therapeutics. Life Sciences. 2023; 335: 122249.
[24] Chen Y, Dong K, Fang C, Shi H, Luo W, Tang CE, *et al*. The predictive values of monocyte-lymphocyte ratio in postoperative acute kidney injury and prognosis of patients with Stanford type A aortic dissection. Frontiers in Immunology. 2023; 14: 1195421.
[25] Al-Rifai R, Vandestienne M, Lavillegrand JR, Mirault T, Cornebise J, Poisson J, *et al*. JAK2V617F mutation drives vascular resident macrophages toward a pathogenic phenotype and promotes dissecting aortic aneurysm. Nature Communications. 2022; 13: 6592.
[26] Zhang B, Zeng K, Guan RC, Jiang HQ, Qiang YJ, Zhang Q, *et al*. Single-Cell RNA-Seq Analysis Reveals Macrophages Are Involved in the Pathogenesis of Human Sporadic Acute Type A Aortic Dissection. Biomolecules. 2023; 13: 399.
[27] Li X, Liu D, Zhao L, Wang L, Li Y, Cho K, *et al*. Targeted depletion of monocyte/macrophage suppresses aortic dissection with the spatial regulation of MMP-9 in the aorta. Life Sciences. 2020; 254: 116927.
[28] Song M, Deng L, Shen H, Zhang G, Shi H, Zhu E, *et al*. Th1, Th2, and Th17 cells are dysregulated, but only Th17 cells relate to C-reactive protein, D-dimer, and mortality risk in Stanford type A aortic dissection patients. Journal of Clinical Laboratory Analysis. 2022; 36: e24469.
[29] Ye J, Wang Y, Wang Z, Ji Q, Huang Y, Zeng T, *et al*. Circulating Th1, Th2, Th9, Th17, Th22, and Treg Levels in Aortic Dissection Patients. Mediators of Inflammation. 2018; 2018: 5697149.
[30] Hou Y, Li Y, Liu B, Wan H, Liu C, Xia W. Research Progress on B Cells and Thoracic Aortic Aneurysm/Dissection. Annals of Vascular Surgery. 2022; 82: 377–382.
[31] Gao H, Sun X, Liu Y, Liang S, Zhang B, Wang L, *et al*. Analysis of Hub Genes and the Mechanism of Immune Infiltration in Stanford Type a Aortic Dissection. Frontiers in Cardiovascular Medicine. 2021; 8: 680065.
[32] Zhang H, Chen T, Zhang Y, Lin J, Zhao W, Shi Y, *et al*. Crucial Genes in Aortic Dissection Identified by Weighted Gene Coexpression Network Analysis. Journal of Immunology Research. 2022; 2022: 7585149.
[33] Damiani D, Tiribelli M. ABCG2 in Acute Myeloid Leukemia: Old and New Perspectives. International Journal of Molecular Sciences. 2023; 24: 7147.
[34] Kukal S, Guin D, Rawat C, Bora S, Mishra MK, Sharma P, *et al*. Multidrug efflux transporter ABCG2: expression and regulation. Cellular and Molecular Life Sciences. 2021; 78: 6887–6939.
[35] Sarkadi B, Homolya L, Hegedűs T. The ABCG2/BCRP transporter and its variants - from structure to pathology. FEBS Letters. 2020; 594: 4012–4034.
[36] Yuan Y, Yang Z, Miao X, Li D, Liu Z, Zou Q. The clinical significance of FRAT1 and ABCG2 expression in pancreatic ductal adenocarcinoma. Tumour Biology. 2015; 36: 9961–9968.
[37] Xu R, Tan H, Zhang J, Yuan Z, Xie Q, Zhang L. Fam20C in Human Diseases: Emerging Biological Functions and Therapeutic Implications. Frontiers in Molecular Biosciences. 2021; 8: 790172.
[38] Liu X, Zhan Y, Xu W, Liu X, Geng Y, Liu L, *et al*. Prognostic and immunological role of Fam20C in pan-cancer. Bioscience Reports. 2021; 41: BSR20201920.
[39] Wang Z, Pascal LE, Chandran UR, Chaparala S, Lv S, Ding H, *et al*. ELL2 Is Required for the Growth and Survival of AR-Negative Prostate Cancer Cells. Cancer Management and Research. 2020; 12: 4411–4427.
[40] Park KS, Bayles I, Szlachta-McGinn A, Paul J, Boiko J, Santos P, *et al*. Transcription elongation factor ELL2 drives Ig secretory-specific mRNA production and the unfolded protein response. Journal of Immunology. 2014; 193: 4663–4674.
[41] Swaminathan B, Thorleifsson G, Jöud M, Ali M, Johnsson E, Ajore R, *et al*. Variants in ELL2 influencing immunoglobulin levels associate with multiple myeloma. Nature Communications. 2015; 6: 7213.
[42] Li Y, Chen Z, Cui J, Yu J, Niu Y, Ran S, *et al*. MTHFD2 ablation in T cells protects against heart transplant rejection by perturbing IRF4/PD-1 pathway through the metabolic-epigenetic nexus. The Journal of Heart and Lung Transplantation. 2023; 42: 1608–1620.
[43] Sugiura A, Andrejeva G, Voss K, Heintzman DR, Xu X, Madden MZ, *et al*. MTHFD2 is a metabolic checkpoint controlling effector and regulatory T cell fate and function. Immunity. 2022; 55: 65–81.e9.
[44] Bai R, Wu D, Shi Z, Hu W, Li J, Chen Y, *et al*. Pan-cancer analyses demonstrate that ANKRD6 is associated with a poor prognosis and correlates with M2 macrophage infiltration in colon cancer. Chinese Journal of Cancer Research. 2021; 33: 93–102.
[45] Xia Y, Xu Y, Liu Q, Zhang J, Zhang Z, Jia Q, *et al*. Glutaredoxin 1 regulates cholesterol metabolism and gallstone formation by influencing protein S-glutathionylation. Metabolism: Clinical and Experimental. 2023; 145: 155610.
[46] Andreadou I, Efentakis P, Frenis K, Daiber A, Schulz R. Thiol-based redox-active proteins as cardioprotective therapeutic agents in cardiovascular diseases. Basic Research in Cardiol-

ogy. 2021; 116: 44.
[47] Chang Y, Li G, Zhai Y, Huang L, Feng Y, Wang D, *et al*. Redox Regulator *GLRX* Is Associated With Tumor Immunity in Glioma. Frontiers in Immunology. 2020; 11: 580934.
[48] Chopra S, Trepka K, Sakhamuri S, Carretero-González A, Zhu J, Egusa E, *et al*. Theranostic Targeting of CUB Domain-Containing Protein 1 (CDCP1) in Multiple Subtypes of Bladder Cancer. Clinical Cancer Research. 2023; 29: 1232–1242.
[49] Bartkowiak K, Mossahebi Mohammadi P, Gärtner S, Kwiatkowski M, Andreas A, Geffken M, *et al*. Detection and Isolation of Circulating Tumor Cells from Breast Cancer Patients Using CUB Domain-Containing Protein 1. Journal of Proteome Research. 2023; 22: 1213–1230.
[50] Lun Y, Borjini N, Miura NN, Ohno N, Singer NG, Lin F. CDCP1 on Dendritic Cells Contributes to the Development of a Model of Kawasaki Disease. Journal of Immunology. 2021; 206: 2819–2827.
[51] Chen F, Han J, Tang B. Patterns of Immune Infiltration and the Key Immune-Related Genes in Acute Type A Aortic Dissection in Bioinformatics Analyses. International Journal of General Medicine. 2021; 14: 2857–2869.
[52] Lian R, Zhang G, Yan S, Sun L, Zhang G. Identification of Molecular Regulatory Features and Markers for Acute Type A Aortic Dissection. Computational and Mathematical Methods in Medicine. 2021; 2021: 6697848.